

## Microscale analysis of metal uptake by argillaceous rocks using positive matrix factorization of microscopic X-ray fluorescence elemental maps

János Osán<sup>1\*</sup>, Annamária Kéri<sup>1</sup>, Dániel Breitner<sup>1</sup>, Margit Fábrián<sup>1</sup>, Rainer Dähn<sup>2</sup>, Rolf Simon<sup>3</sup>, Szabina Török<sup>1</sup>

<sup>1</sup> Hungarian Academy of Sciences, Centre for Energy Research, P.O. Box 49, H-1525 Budapest, Hungary

<sup>2</sup> Laboratory for Waste Management, Paul Scherrer Institute, 5232 Villigen PSI, Switzerland

<sup>3</sup> Karlsruhe Institute of Technology, Institute for Synchrotron Radiation, Hermann-von-Helmholtz-Platz 1, D-76344 Eggenstein-Leopoldshafen, Germany

\*Corresponding author: e-mail: [janos.osan@energia.mta.hu](mailto:janos.osan@energia.mta.hu)

### Abstract

Argillaceous rocks are considered in most European countries as suitable host rock formations for the deep geological disposal of high-level radioactive waste (HLW). The most important chemical characteristic in this respect is their generally strong radionuclide retention property due to the high sorption capacity. Consequently, the physico-chemical parameters of these processes have to be studied in great detail. Synchrotron radiation microscopic X-ray fluorescence (SR  $\mu$ -XRF) has sufficient sensitivity to study these processes on the microscale without the necessity of the application of radioactive substances. The present study focuses on the interaction between the escaped ions and the host-rock surrounding the planned HLW repository. SR  $\mu$ -XRF measurements were performed on thin sections subjected to sorption experiments using 5  $\mu$ m spatial resolution. Inactive Cs(I), Ni(II), Nd(III) and natural U(VI) were selected for the experiments chemically representing key radionuclides. The thin sections were prepared on high-purity silicon wafers from geochemically characterized cores of Boda Claystone Formation, Hungary. Samples were subjected to 72-hour sorption experiments with one ion of interest added. The  $\mu$ -XRF elemental maps taken usually on several thousand pixels indicate a correlation of Cs and Ni with Fe- and K-rich regions suggesting that these elements are predominantly taken up by clay-rich phases. U and Nd was found to be bound not only to the clayey matrix, but the cavity filling minerals also played important role in the uptake. Multivariate methods were found to be efficient tools for extracting information from the elemental distribution maps even when the clayey matrix and fracture infilling regions were examined in the same measured area. By using positive matrix factorization as a new approach the factors with higher sorption capacity could be identified and with additional mineralogical information the uptake capacity of the different mineral phases could be quantified. The results were compared with cluster analysis when the regions dominated by different mineral phases are segmented. The multivariate approach based on  $\mu$ -XRF to identify the minerals was validated using microscopic X-ray diffraction.

**Keywords:** micro-XRF; sorption; positive matrix factorization; radioactive waste; argillaceous rock

### 1. Introduction

In most European countries, clay-rich rocks are considered as suitable host rock formations for isolation of the radionuclides generated by the nuclear industry from the biosphere for thousands of years. During this time period the radionuclides might migrate from the engineered barriers and the safety is determined by the retention capability of the host rock. Following water intrusion into the repository, radionuclide contaminants can be released. Clay rocks have very good retention capability due to their high sorption capacity. Sorption depends on the water/solid compositions, porewater properties such as pH and Eh, as well as the presence of complexing anions as they determine the radionuclide chemical speciation. The interaction of radioactive ions with clay minerals has been thoroughly studied in the past [1, 2, 3]. Nowadays, most attempts to quantify the retention function are focused on the measurement of distribution ratios ( $K_d$ ) between the mobile and stationary phase [4, 5,

6]. These experiments are necessary but will not give the final answer to the questions: which minerals retain the radionuclides and how reversible the processes are (type of chemical bonds involved). With the revolutionary development of X-ray sources (synchrotrons) and optics such questions can be answered by micro scale resolution spectroscopy and diffraction techniques [7, 8, 9, 10, 11]. A recent review emphasizes the relevance of versatile micro- and nanoanalytical techniques for actinide environmental research [12].

Microscopic X-ray fluorescence ( $\mu$ -XRF) spectroscopy combined with microscopic X-ray diffraction ( $\mu$ -XRD) is a unique possibility to study these highly heterogeneous rocks [10, 13]. The samples and the sorption concentrations must be in the good analytical performance domain of the used techniques. Geological samples are most often studied with microscopy techniques using petrographic thin sections prepared from the rocks of interest. Sorption experiments involving thin sections have to be designed in order to model the chemical conditions present at the depth of the planned repository. Also, the concentrations of the elements of interest in the solutions involved should be sufficiently low in order to avoid precipitation. For this reason, the element of interest after sorption experiment will be present in minor or trace concentration level heterogeneously distributed in the sample. Due to its high dynamic range,  $\mu$ -XRF is a suitable tool to detect simultaneously the distribution of the sorbed elements of interest and elements corresponding to rock-forming minerals. Especially excitation using synchrotron radiation (SR) offers a lateral resolution of 5  $\mu\text{m}$  or better, in the same dimension as heterogeneities in the studied rocks. It is also advantageous that the key radionuclides representing transuranium elements, fission and corrosion products that are not present in the rock can be substituted with inactive or natural analogues without requiring high activity radioisotopes for microscopic sorption studies.

Although SEM/EDX is well suited for determination of major elements in thin sections, the usually applied high vacuum can cause dehydration and collapse in clay mineral structure [14, 15] hindering additional studies of the uptake mechanism on the same samples. The low-vacuum version of the method, however, suffers from limited quantitativity. Powder  $\mu$ -XRD has limitation as well in phase determination because oriented crystals comparable to the beam size can be present in the samples of interest. The presence of oriented crystals can yield erroneous crystalline composition by  $\mu$ -XRD since some representative reflections can be missing from the diffractograms.

Two-dimensional scanning of a selected area using  $\mu$ -XRF results in a large data matrix with dimensions  $n_{el} \times n_x \times n_y$ , where  $n_{el}$  is the number of analyzed elements,  $n_x$  and  $n_y$  are the number of scanned pixels horizontally and vertically, respectively. Even though  $\mu$ -XRF performed in air is not capable of detecting major light elements (O, Na, Mg, Al), information on the mineral phases responsible for the uptake of the radionuclide of interest can be derived from the data set if suitable mathematical methods are applied for data treatment. The assumptions derived from  $\mu$ -XRF can be verified using  $\mu$ -XRD phase analysis at representative selected positions [10, 13].

One possibility is to examine inter-elemental correlations through scatter plots of the X-ray intensities of two selected elements. The connection of the element of interest to a given mineral phase can be judged based on the similarity of the correlation between two elements representative for the mineral phase and the correlation between each of these elements and the element of interest. The single value of the correlation coefficient bears insufficient information since more mineral phases can be present in the scanned area. Due to differences in sample thickness and matrix composition, the position of the points in the scatter plot can deviate from the expected straight line, even if the concentration ratio of the two elements is constant, which has to be taken into account [16, 17].

Other possibility is to apply multivariate methods such as principal component analysis (PCA) or factor analysis (FA). These methods are generally used for analysis of large data sets. However, the expression of factors in the original variables (factor loadings) can contain negative values expressing anticorrelation with original variables (chemical elements). This problem can be overcome by using positive matrix factorization (PMF), since the factor loadings (called as factor profiles in PMF) are forced to be positive. PMF is commonly used in air pollution studies where factors representing sources are derived from the time variation of pollutant concentrations [18,19,20]. PMF was successfully applied to process three-dimensional datasets, e.g. distribution maps from Raman imaging [21]. However, no applications of PMF to scanning  $\mu$ -XRF datasets have been reported to date.

Segmentation of the data set can be performed using cluster analysis, based on the similarity (distance) of the pixels in the abstract space defined by elemental X-ray intensities. The most commonly used method is the non-hierarchical K-means clustering algorithm. Instead of using the original variables (elemental intensities), PCA pretreatment can be useful, where clustering is performed in a space with reduced dimensions [22, 23, 24].

The aim of the present study was to evaluate the combination of  $\mu$ -XRF and multivariate methods especially PMF as a new mathematical approach for application in sorption studies involving argillaceous rock thin sections in order to obtain quantitative information on the sorption capacity of the mineral phases responsible for the uptake. The presence of the phases predicted by  $\mu$ -XRF was verified by  $\mu$ -XRD. The performance of the combined method is discussed on thin clay rock sections subjected to sorption experiments, using inactive Cs(I), Ni(II), Nd(III) and natural U(VI), chemically representing fission and corrosion products as well as transuranium elements of interest.

## **2. Materials and Methods**

### **2.1. Samples**

The rocks investigated were prepared from geochemically characterized cores from drillings in Boda Claystone Formation (BCF), considered as a possible formation for high-level radioactive waste (HLW) repository in Hungary. The Upper Permian sedimentary sequence of the BCF is located in Western Mecsek Mountains, SW Hungary. The sediments of the BCF are dominantly red and reddish brown in colour, reflecting the oxidizing nature of the depositional and early diagenetic environments. The BCF was deposited in a shallow-water salt lake environment surrounded by dry to saline mudflat, under semi-arid to arid climatic conditions [25, 26, 27, 28]. Two distribution areas of BCF are known in West-Mecsek Mountains, the perianticlinal structure of the West-Mecsek Anticline (WMA) Block and the Gorica Block (GB) [28].

The main rock-forming minerals of the BCF are: clay minerals (mainly illite and chlorite), authigenic albite, analcime (GB only), detrital quartz, carbonate minerals (calcite and dolomite) and hematite [29, 30]. The rocks are highly heterogeneous on the microscale, two major regions can be distinguished, the clayey matrix and the fracture infillings. High amount of clay minerals (around 50 m/m% phyllosilicates, mainly illite-muscovite, chlorite, kaolinite and mixed structure clay minerals) as well as albite cement (and analcime cement for GB) form the clayey matrix. The most important clay mineral is illite, containing potassium and iron. Nanoscale hematite flakes were detected between illite plates by transmission electron microscopy [31]. The fracture infillings contain mostly authigenic albite (or analcime for GB), carbonate minerals (calcite and dolomite) and authigenic potassium feldspar. The absolute dominant rock type of the formation is albitic claystone in the WMA Block and albite- and analcime-bearing claystone in the Gorica Block [32].

Representative core samples were selected from both blocks for preparation of thin sections. Small pieces of selected core samples from GB (sample Ib-4) and WMA (sample D-11) were grinded and mounted onto 350- $\mu$ m thick high purity silicon wafers and polished by 0.25  $\mu$ m diamond paste. The average thicknesses of the sections were 50  $\mu$ m. Samples were subjected to 24–72 hour sorption experiments with one ion of interest added, using synthetic porewater for Cs and Ni, and a 0.1 M NaCl solution for Nd and U as background electrolyte. The NaCl solution was applied due to solubility constraints to ensure a sufficient loading of the element of interest to match the sensitivity of  $\mu$ -XRF while avoiding precipitation in the solution itself.

### **2.2 Microscopic XRF/XRD measurements**

The experiments were performed at the FLUO beamline of ANKA. The white beam of a bending magnet was monochromatized by a W/Si multilayer double monochromator. A silicon-drift detector was used to collect fluorescence spectra. The  $\mu$ -XRF elemental mapping measurements were performed at a primary beam energy of 17.5 keV ( $\Delta E/E = 10^{-2}$ ), using a compound refractive lens for focusing a beam down to a spot size of  $2 \times 5 \mu\text{m}^2$ . Elemental maps were recorded for the adsorbed element (Cs, Ni, Nd, U) as well as for the major and minor elements of the rock measurable by XRF (e.g. K, Ca, Fe, Rb, Sr), using a 5  $\mu$ m step size and 4–10 s counting time per pixel. The net characteristic X-ray intensities were determined by processing of the full X-ray spectra collected at each pixel using the AXIL software [33]. The elemental maps served as a basis for investigating correlation between the sorbed element and elements representative for particular distinct minerals.

The elemental concentrations were calculated using the fundamental parameter method, taking into account the thickness of the sample (50  $\mu\text{m}$ ) and the average density of the rock (2.7  $\text{g}/\text{cm}^3$ ). The excitation intensity and the geometrical factor were determined from measurements of the NIST SRM 613 standard reference material in identical conditions. The X-ray spectra recorded in air and a 17.5 keV excitation energy do not contain information about elements with lower atomic number than potassium therefore the following assumptions were considered about the residual matrix: the main component of the sample is aluminosilicate (considered in the form of  $\text{Al}_2\text{O}_3\cdot\text{SiO}_2$ ), potassium and iron occur in oxide form ( $\text{K}_2\text{O}$ ,  $\text{Fe}_2\text{O}_3$ ), while calcium is present in the carbonate form ( $\text{CaCO}_3$ ).

Several  $\mu\text{-XRD}$  images were collected by a 130 mm diameter CCD detector from selected positions of interest. The calibration for the  $\mu\text{-XRD}$  measurements was performed by measurements of standards (corundum, silicon,  $\text{PbCO}_3$  and  $\text{Pb}(\text{OH})_2$ ). The beam position on the XRD images was determined using the XRDUA software [34]. The least distorted circular rings were obtained using the parameters of  $-5^\circ$  tilt and  $25^\circ$  rotation. The phase identification and quantification was carried out employing the XDB software [35]. This software allows for full interpretation of a sample diffractogram and helps generate initial concentrations of identified minerals based on a standardless approach. With the mass balance procedure on the XDB software helped to refine the final phase composition. After the phase identification, we calculate the quantitative phase composition. The quantitative calculations are based on the reference intensity method, therefore it needs the reference intensity -  $I/I_c$  - for each phase. The reliability of the results greatly depends on the distribution of the intensities to the identified phases. Phase proportions are derived from the weight parameters of the profile fit corrected with their respective  $I/I_c$  coefficient. The calculated phase proportions depend on the particle size of the components and the absolute amounts (phase percentages) are normalized to the sum of the phases.

### 2.3 Multivariate methods

Multivariate data analysis methods are used in several areas of environmental chemistry in order to handle large scale data matrices. The aim of their application is to get new information from the estimation of the number and composition of factors (latent variables) describing the dataset. Many multivariate methods are known from which factor analysis (FA), positive matrix factorization (PMF) and cluster analysis (CA) were tested in this work. Since all multivariate methods work with two-dimensional matrices (variables–observations), the 2D elemental maps for each element (variable) were unfolded to 1D vectors. The resulting factor maps or cluster maps were created after refolding the resulting data to 2D matrices.

Standard FA employing varimax rotation was performed in this work using the software package IDAS [36]. The number of factors present in the dataset was determined using the 95% limit of the explained variance. The intensity values were scaled using autoscaling (z-transformation; Eqn 1) in order to take the variables into consideration with similar weights but assigning higher weight to data with smaller statistical error [37]:

$$z_{ij} = \frac{x_{ij} - \bar{x}_j}{s_j} \quad (1)$$

where  $\bar{x}_j$  is the average of the measurement results connected to the given variable  $j$  and  $s_j$  is the corresponding standard deviation.

PMF decomposes the data matrix to two non-negative matrices in the following way:

$$\mathbf{E}_{ij} = \mathbf{X}_{ij} - \mathbf{Y}_{ij} = \mathbf{X}_{ij} - \sum_{h=1}^p \mathbf{G}_{ih} \mathbf{F}_{hj} \quad (2)$$

where  $\mathbf{E}$  is the residual matrix,  $\mathbf{Y}$  is the model matrix,  $\mathbf{X}$  is the input data matrix with  $i$  number of sampling points and  $j$  number of variables,  $\mathbf{G}$  and  $\mathbf{F}$  are the left and right factor matrices and  $p$  is the number of factors [38].

The best PMF decomposition can be obtained by the minimizing the objective function and choosing the values of  $\mathbf{G}$  and  $\mathbf{F}$  as non-negative:

$$Q(\mathbf{E}) = \sum_{i=1}^n \sum_{j=1}^m \left( \frac{x_{ij} - \sum_{k=1}^p g_{ik} f_{kj}}{\sigma_{ij}} \right)^2 \quad (3)$$

where  $\sigma_{ij}$  are the uncertainty of each data point [38].

It can be seen from Eqn 3 that the method uses the uncertainty of the measured values for the proper weighting of the data matrix thus allowing the separate treatment of the matrix elements. As a consequence values measured under the detection limit can also be taken into the dataset thus avoiding data loss if the uncertainties are also given. In addition of weighting it is also different from standard factor analysis that the factors are not orthogonal to each other.

In this work the EPA PMF 3.0 software package was used for performing the calculations [38]. The software uses multistage iteration method to solve the PMF problem starting from pseudorandom initial values, therefore the number of factors and runs were given as input parameters. The number of factors was assumed for each dataset from FA results of the same set of elemental maps. Elements were categorized in three different groups based on the signal-noise ratio of their intensities. Elements with high signal-to-noise ratio were categorized as “strong”, including every element that could possibly be a component of mineral phases occurring in the sample, as well as the element added in the sorption experiment. Elements with small intensities and high uncertainties (e.g. Pb, Cu) were in the group of “weak”. Elements with very noisy distribution maps (e.g. Ga) were classified into “bad” category and were not taken into account during the evaluation. The output factor profiles were calculated by the software considering that the average factor contribution is equal to unity. However, in the present case, the factor contribution cannot be higher than one at each measured pixel, therefore the output factor profiles were maximum normalized.

Non-hierarchic CA is generally applied for data matrices containing numerous measurement points [37]. In this work the  $k$ -means algorithm was used that classifies every object (measurement point) to a cluster whose centroid is the closest to the given object. CA was performed using the built-in routine of IDL or using the IDAS software [36].

### 3. Results and Discussion

#### 3.1. Inter-elemental correlations

##### *Effect of general mineral composition*

To identify the minerals on the microscale at first the elemental maps were studied. In general, high correlation could be observed between potassium and iron on the elemental distribution maps and K–Fe correlation diagrams for samples Ib-4 (from Gorica block) and D-11 (from West-Mecsek Anticline) as well. The reason is the presence of illite, the main clay mineral containing on average 6.03 m/m% potassium and 1.43 m/m% iron [39]. This correlation was even enhanced in BCF samples by the observed nanometre size (<200 nm) hematite grains wedged between illite trusses [28,31]. The two mineral phases could not be separated in a single pixel by  $\mu$ -XRF using a beam size of  $3 \times 5 \mu\text{m}^2$ . Both mineral phases contributed to the measured intensity of the two elements therefore it increased their correlation. The areas where potassium and iron were present together were considered as clayey matrix containing phyllosilicates (mainly illite), fine grained albite, rutile and nanocrystalline hematite.

In some sample areas the K–Fe correlation was generally decreased due to the presence of larger hematite grains with sizes of the order of the pixels. These high intensity points can be seen as hotspots on the iron elemental maps. Larger iron-oxide minerals can appear as outlying points on the correlation diagram (Fig. 1).

Fracture infilling carbonate may not be present only in the form of calcite but Mg- and Mn-carbonate may occur as well.  $\mu$ -XRF performed in air is unable to detect magnesium because of its low-energy K-lines. The presence of Mn-carbonate could only be inferred indirectly from the examination of elemental maps and Ca–Mn correlation diagrams (Fig. 2), when calcium and manganese were found to be together.

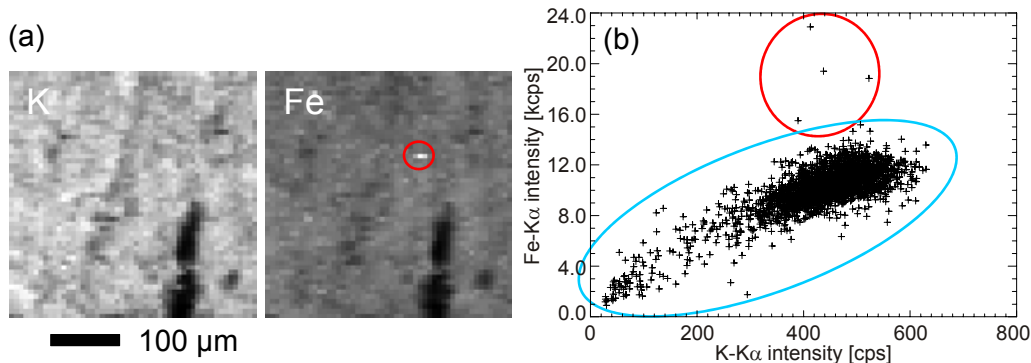


**Figure 1.** Elemental maps of potassium and iron from an area of  $0.35 \times 0.35 \text{ mm}^2$  on a thin section prepared from sample D-11 (a). The elemental maps are presented as max-min normalized, black representing the minimum and white the maximum intensity. High intensity iron points could be observed on the framed area. K–Fe correlation diagram corresponding to the area (b) ( $r_{K-Fe} = 0,758$ ), points circled in blue imply correlation, points circled in red are outliers

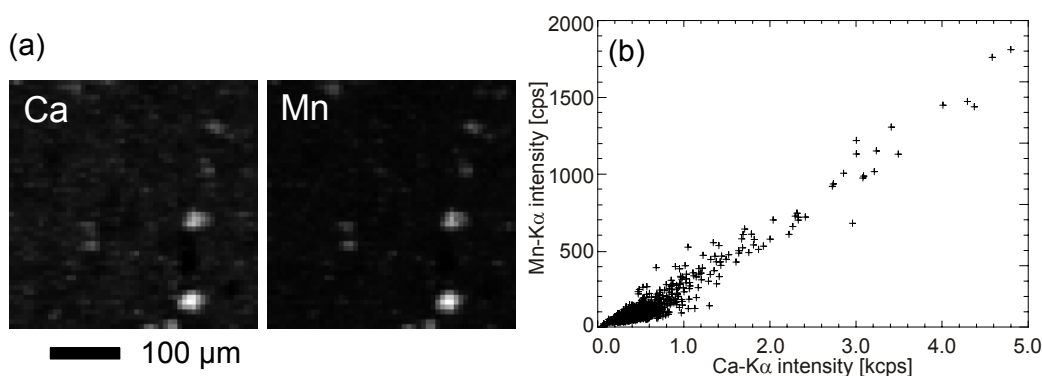


**Figure 2.** Calcium and manganese elemental maps from an area of  $0.35 \times 0.35 \text{ mm}^2$  on a thin section prepared from sample D-11 (a), and the corresponding Ca–Mn correlation diagram (b) ( $r_{Ca-Mn} = 0,939$ )

In certain areas of sample D-11 the Ca–Mn correlation coefficient was found to be low. However, it is clearly visible on the corresponding correlation diagram that two different Ca–Mn intensity ratios can be fitted to the measurement points (Fig. 3), implying the presence of (at least) two-phase carbonate.

The reason of the genesis of the different carbonates is that the composition of the solutions flowing in the rifts was changing. Consequently the composition of the formed minerals became also different. The presence of the multi-generational carbonates was also confirmed by the former cathodoluminescence measurements [31]. Calcium-containing minerals are single crystals on this microscale that can hamper the quantitative phase analysis using powder  $\mu$ -XRD.

For some scanned areas of the D-11 sample, a quite low value of K–Fe correlation coefficient was observed (e.g.  $r=0.032$ , see Fig. 4). The reason for it is the low Fe-K $\alpha$  intensities with corresponding high K-K $\alpha$  intensities on certain areas that can be seen on the elemental maps and on the K–Fe correlation diagrams (Fig. 4). In addition to the presence of calcite, significant amount of potassium feldspar, another cavity filling mineral could be concluded as present [31]. It could also be observed on the correlation diagram where three sets of points can be distinguished. The outlier points with constant K-K $\alpha$  intensity were caused by micrometer-size hematite grains. The remaining two sets of points were caused by potassium feldspar and illite. While a straight line with a positive slope can be fitted to the former, the latter points are located at a nearly horizontal line. The nearly zero slope linear relation shows the different K-K $\alpha$  intensity of the potassium feldspar with nearly constant Fe-K $\alpha$  intensity. The phenomenon could be explained by the different quantity of the mineral filling out the excitation volume of the given pixel.

There were some areas on the sample where the intensity of every studied element was low (Fig. 4). In these areas only minerals that cannot be detected by  $\mu$ -XRF because of their low atomic number element content (Na, Mg, Si, O) were present. Typical such minerals are albite and quartz [31].

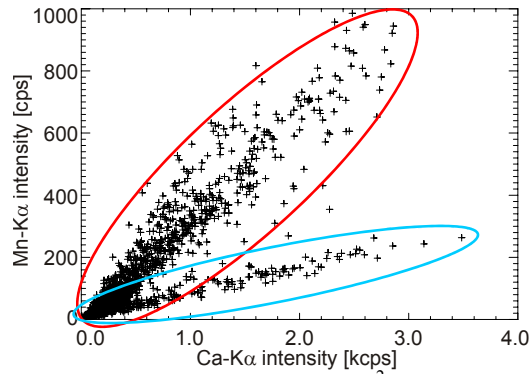


**Figure 3.** Ca–Mn scatter plot from a sample area of  $0.25 \times 0.3 \text{ mm}^2$  on a thin section prepared from sample D-11 ( $r_{Ca-Mn} = 0,878$ ). Straight lines with different slopes can be fitted to the points circled with different colours

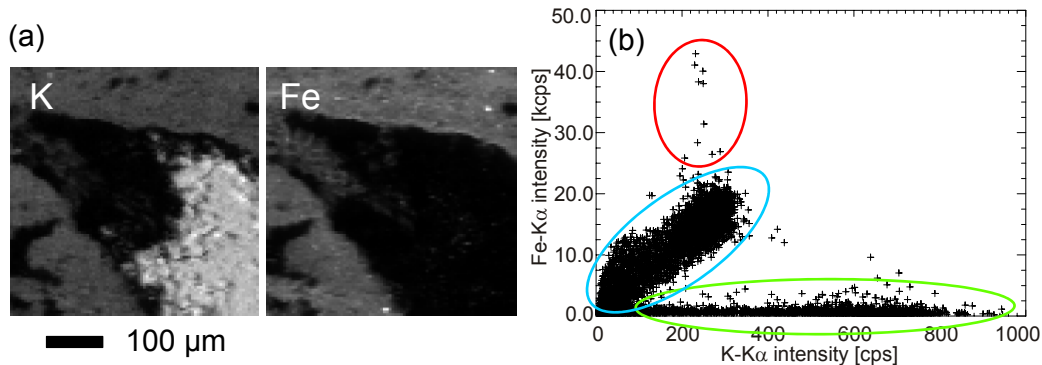


**Figure 4.** Elemental maps for a sample area of  $0,45 \times 0,45 \text{ mm}^2$  on a D-11 thin section (a) and the corresponding K–Fe scatter plot (b) ( $r_{K-Fe} = 0.032$ ); straight lines of different slopes can be fitted to the set of points circled with different colours

Based on the pairwise elemental correlations, the role of three groups of mineral phases in the uptake of ions involved in the sorption experiment can already be judged. If the element of interest is well correlated with both K and Fe, it can be assumed to be taken up by the clayey matrix.

If the element of interest is well correlated with Ca and Mn, it can be assumed to be connected to the carbonates, however if the element of interest shows anticorrelation with both K and Ca, it can be connected to albite or analcime phases in the given rock.

#### *Effect of uptake of ions*

Based on the above simple approach the sorbing mineral can be identified in many cases. For every measured sample the intensity of nickel and cesium showed the strongest correlation with the clayey matrix that could be deduced by correlation between the given element and K as well as Fe (Fig. 5). It could be observed for uranium and neodymium that they did not only bind on the clayey matrix. For this reason the investigation of the cavity filling minerals was also necessary for the samples treated with  $\text{UO}_2^{2+}$  as well as  $\text{Nd}^{3+}$  ions.

Sample D-11 treated with  $\text{UO}_2^{2+}$  ion have many different properties from the ones described above. In contrast to the samples treated with other ions, significant uranium binding mineral phase exists apart from clayey matrix. Comparing the elemental map of U and Ca (Fig. 6) it could be seen that apart from the clay matrix the  $\text{UO}_2^{2+}$  was bound in rings around the calcium rich phases. Comparing the Fe elemental map to the ones investigated above it could be determined that iron is also enriched in the same rings around the calcium grains. U-rich rings could be seen around Ca-rich phases surrounded with either silicates or with clayey matrix. In the former case, the enrichment of Fe in ring form was visible in the Fe elemental map, while it was not visible in the latter case because of the high iron content of the clayey matrix. The two measured areas referred to secondary mineral phases with significant uranium binding property but they could not be identified by the examination of the elemental maps and correlation diagrams.

Sample Ib-4 treated with  $\text{UO}_2^{2+}$  ion showed different phenomenon compared to the sample D-11 treated the same way since no rings were observed on the U elemental map (Fig. 6).

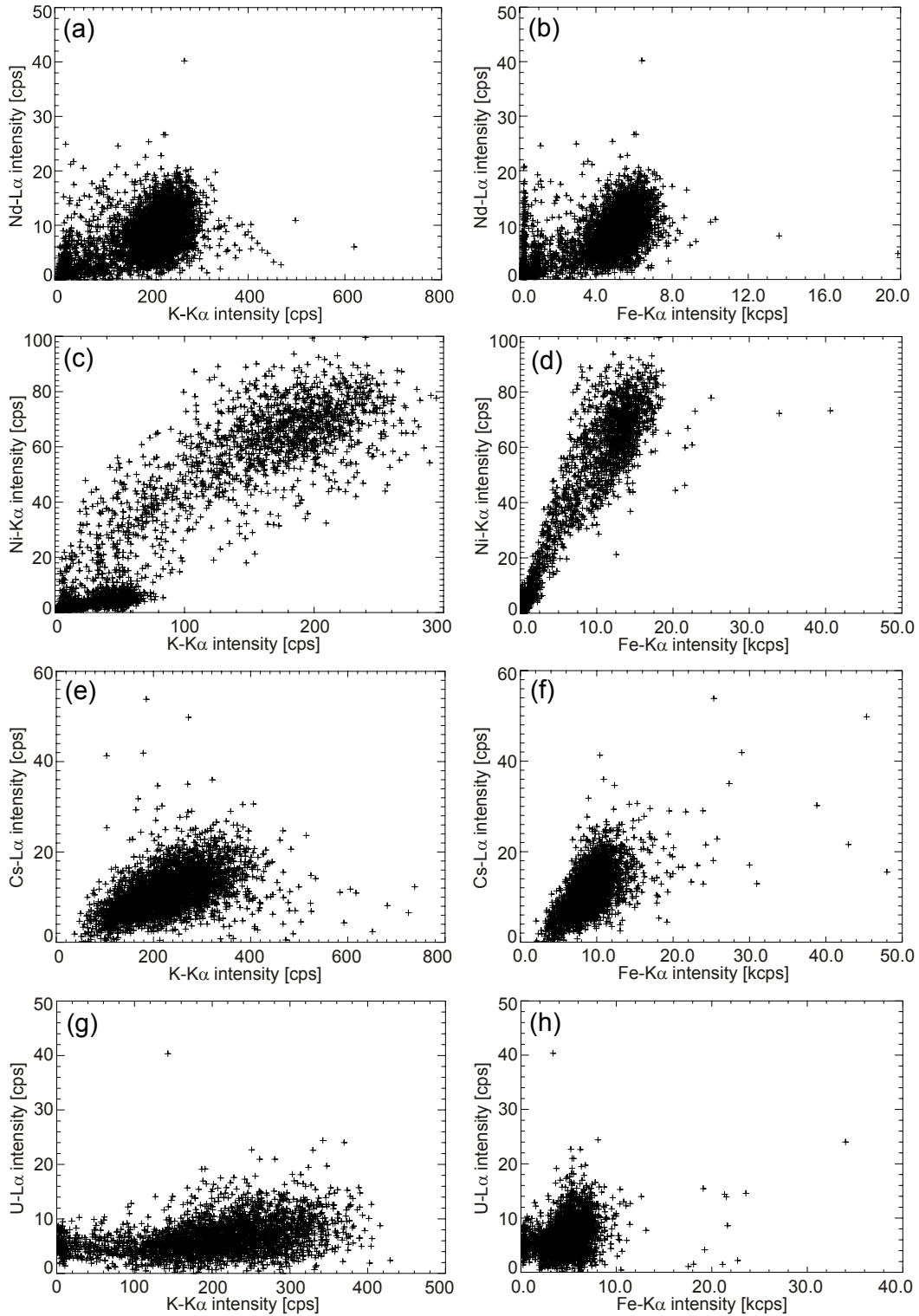


**Figure 5.** Scatter plots of the sorbed element (Nd, Ni, Cs, U) versus elements representative for the clayey matrix (K and Fe), (a) K–Nd ( $r_{K-Nd} = 0.55$ ) and (b) Fe–Nd ( $r_{Fe-Nd} = 0.57$ ) from a  $0.25 \times 0.3 \text{ mm}^2$  scanned area on D-11, (c) K–Ni ( $r_{K-Ni} = 0.95$ ) and (d) Fe–Ni ( $r_{Fe-Ni} = 0.96$ ) from a  $0.2 \times 0.3 \text{ mm}^2$  scanned area on Ib-4, (e) K–Cs ( $r_{K-Cs} = 0.49$ ) and (f) Fe–Cs ( $r_{Fe-Cs} = 0.63$ ) from a  $0.3 \times 0.3 \text{ mm}^2$  scanned area on Ib-4, (g) K–U ( $r_{K-U} = 0.27$ ) and (h) Fe–U ( $r_{Fe-U} = 0.25$ )  $0.3 \times 0.545 \text{ mm}^2$  scanned area on Ib-4

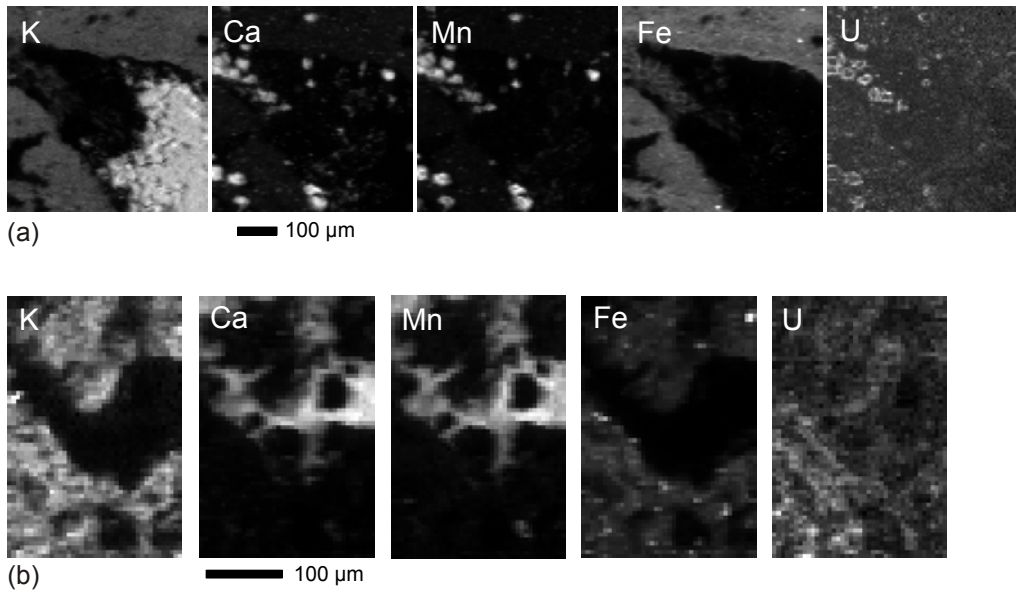


**Figure 6.** Elemental maps of sample areas treated with U, (a) D-11 and (b) Ib-4

These differences point out that the examination of pairwise elemental correlation is a useful tool in identifying the main groups of mineral phases responsible for the uptake, but it works well for simple cases, when one of them binds the majority amount of the element of interest. When the clayey matrix as well as fracture infilling is aimed to be examined from the same dataset, multivariate methods are necessary for extracting the information from the elemental distribution maps. Using these methods, identification of the main mineral phase groups responsible for the uptake and quantitative information on the uptake capacity of dominant phases are expected.

For this reason, factor analysis, positive matrix factorization and cluster analysis were applied to the datasets. The applicability of these methods is discussed below on two typical examples, the first one where mainly the clayey matrix is responsible for the uptake (D-11 sample treated with  $\text{Ni}^{2+}$ , denoted as D11-Ni), and the second one where a newly formed phase was also found to play an important role in the uptake (D-11 sample treated with  $\text{UO}_2^{2+}$ , denoted as D11-U). Optical image and elemental maps are presented in Figure 7. The scanned areas were selected to contain both the clayey matrix and fracture infilling minerals.

### 3.2 Factor analysis

Conventional FA using varimax rotation was performed on the 2D data matrices of net characteristic X-ray intensities after autoscaling. Based on the 95% criterion for the expressed total variance, the dataset of D11-Ni could be explained using six factors, while five factors were necessary for D11-U. The results for factor loadings are presented in Figure 8, the factors are ordered according to the explained variance. Factor 1 shows high correlation (or anticorrelation for negative values) with K, Ti, Fe and Rb, representing the clayey matrix for both cases. While the element of interest involved in the sorption experiment is attached to this factor for D11-Ni with the same loading as K, Fe and Rb, U does not show correlation with the elements of the clayey matrix for D11-U. This already points out the main difference between the two examples, and shows that conventional FA is a useful tool to find out if the element of interest was taken up mainly by the clayey matrix or by fracture infilling minerals. Factor 2 has high positive (or negative) loading of Ca, Mn and Sr in both examples, representing the main fracture infilling carbonate minerals. The further factors are different for the two examples reflecting differences in the distribution of minor and trace elements. Factor 3 for D11-U has the highest loading of U, showing slight correlation with Mn and Fe. It means that a separate factor was formed for the element of interest in the case of D11-U, indicating that its distribution was different from that of the main rock-forming minerals. Although FA already delivers useful information on the possible mineral phases responsible for the uptake, the unambiguous identification would need quantitative information on the elements present in the factor having the highest loading of the element of interest.

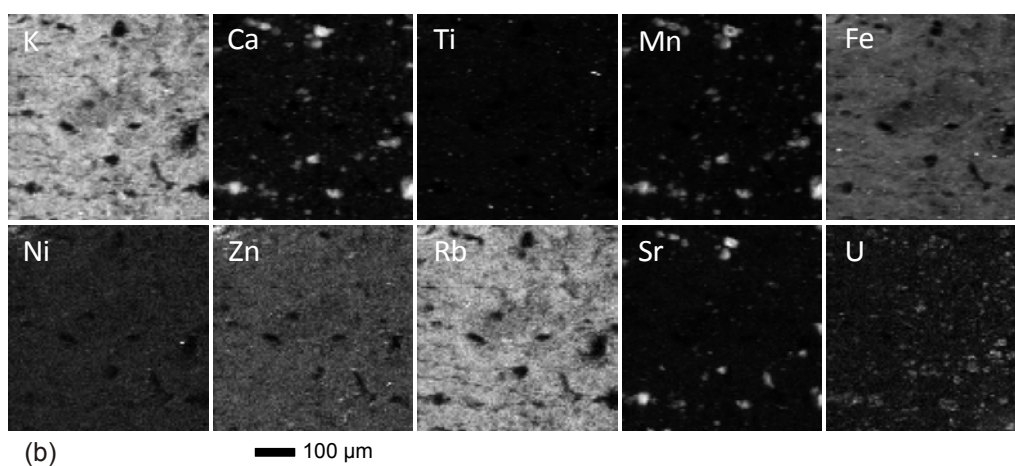
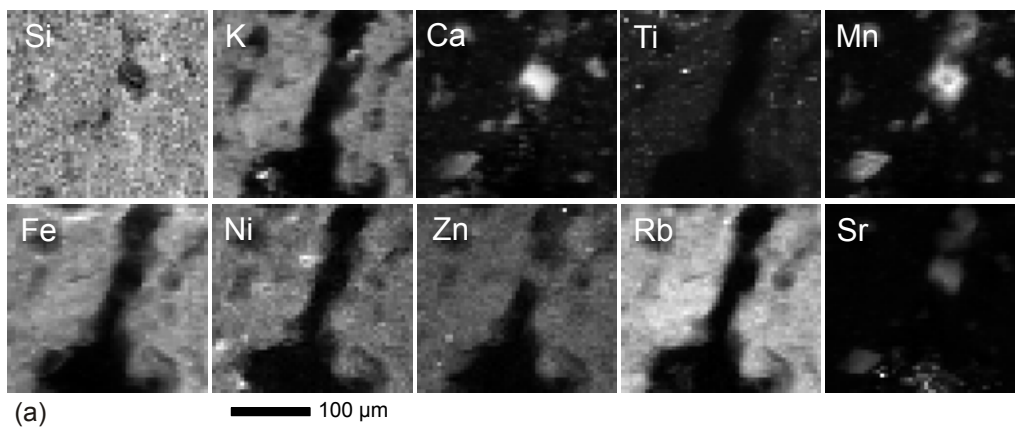


**Figure 7.** Elemental maps for selected areas of D-11 thin sections treated with  $\text{Ni}^{2+}$  (D11-Ni, a) and  $\text{UO}_2^{2+}$  (D11-U, b)

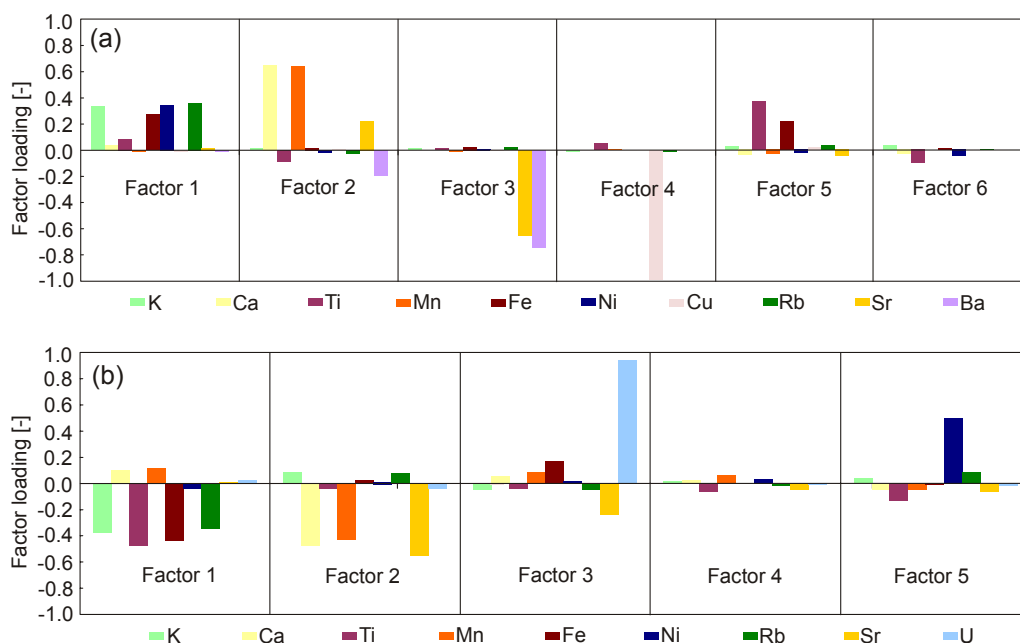


**Figure 8.** Factor loadings for selected areas of sample D11-Ni (a) and D11-U (b) obtained using FA on autoscaled X-ray intensities

The loadings and scores obtained by FA can also contain negative values indicating anticorrelation (Fig. 8), whereof the factor composition could not be easily formed in the measurement points

(pixels). For the quantitative analysis other multivariate statistical methods are necessary that ensure the non-negativity of the factors.

### 3.3 Positive matrix factorization

As a new approach, PMF was performed on the net characteristic X-ray intensity data of different sample areas in order to identify the main components and the mineral phases. The number of factors was assumed to be similar to the results of FA performed for the same dataset. PMF evaluation of elemental maps of scanned areas resulted in the elemental intensity composition of the factors, of which the main (most important) components of the samples could be determined. These are the elements (K, Ca, Ti, Mn, Fe, Rb, Sr) which could be used as a basis for relation of factors to mineral phases. The factor profiles expressed in X-ray intensities were converted to concentrations of the chemical elements using the fundamental parameter method. Final results of the factor distribution of the measurement points (factor contributions) and the composition of the factors in original variables (factor profiles) ( $G$  and  $F$  matrices) for the two selected examples (D11-Ni and D11-U) are presented in Fig. 9.

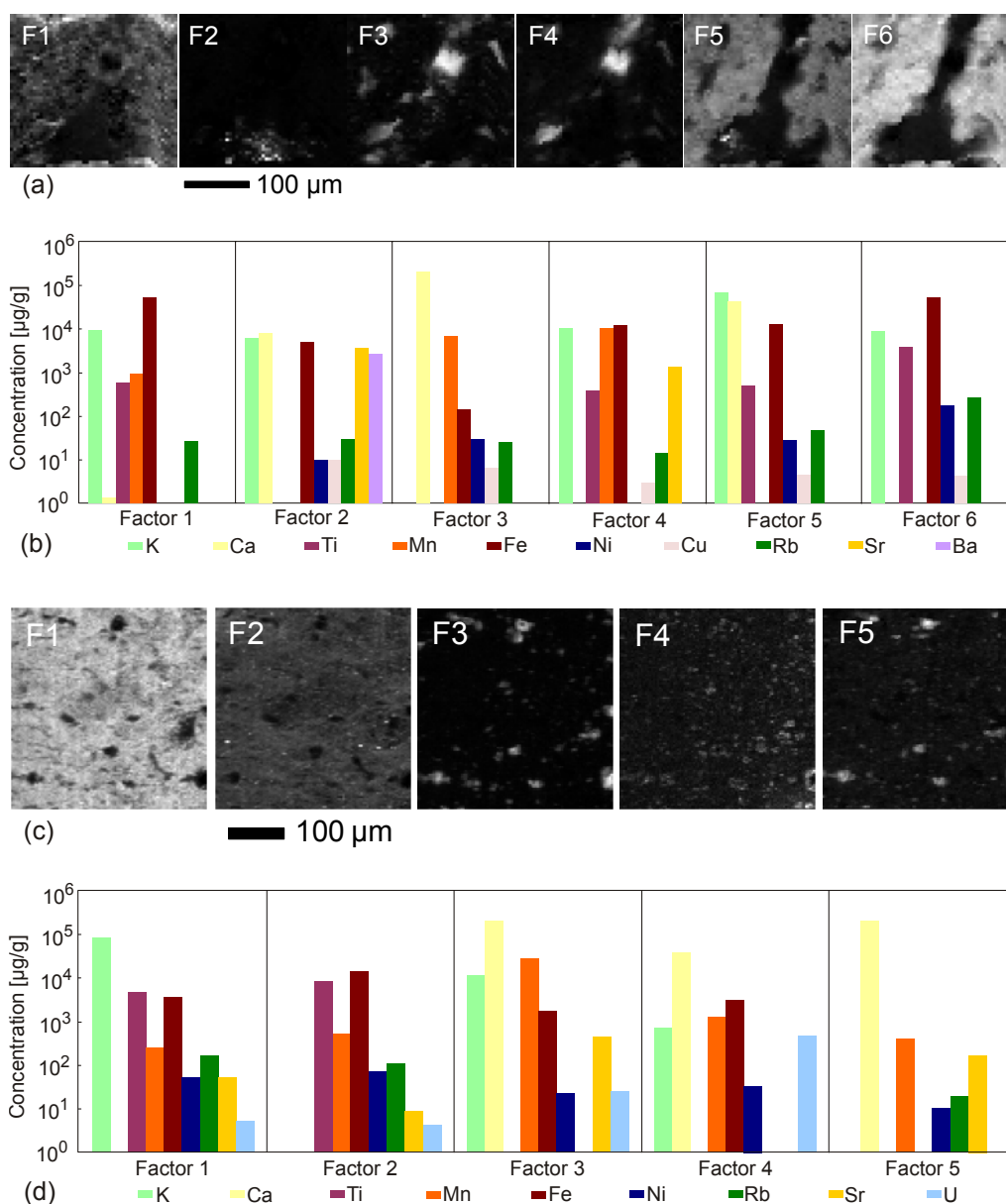


**Figure 9.** Factor contribution maps (a) and profiles expressed as elemental concentrations (b) for selected area of sample D11-Ni and D11-U (c, d). The results were obtained using PMF on X-ray intensities taking into account the corresponding standard deviation in each pixel

From the factor profiles expressed in elemental concentration and from the comparison of the factor distribution maps and the elemental maps information of the mineral phases present could be obtained (see Figs. 7 and 9). For every sample area a factor related to the clayey matrix (Factor 6 for D11-Ni and Factor 3 for D11-U) could be observed containing potassium, iron and titanium in the highest concentration. It could be explained by the presence of the illite trusses and the nanometre size hematite grains wedged between them as well as the presence of the smectite containing calcium and rutile and ilmenite containing titanium. In addition to these elements it also contained a non-negligible amount of rubidium that could integrate in the structure of illite substituting potassium [16].

Calcium-manganese rich mineral phases could also be related to factors by the examination of the factor distribution maps (Factors 3 and 4 for D11-Ni and Factors 3 and 5 for D11-U). Strontium could integrate into the structure of calcite that is verified by the significant strontium content of the factors. Although the distribution maps of the factors were found to be similar to the distribution maps of the corresponding main elements, and the factors could not be identified as single mineral phases, information could be obtained on the elements contained in factors where the element of interest (nickel or uranium in the example scanned areas) is present in elevated concentrations. This information is very valuable for identification of the minerals responsible for the uptake.

The main difference between the two samples is that a separate factor with the contribution map similar to the uranium map was formed for D11-U (Factor 4), while no separate factor was formed for nickel in the case of D11-Ni. In the latter case, nickel was found to be connected to the factor representing the clayey matrix at a concentration of 170  $\mu\text{g/g}$  (the average nickel load of the thin section was 100  $\mu\text{g/g}$ ), in accordance with the around 50% clay content of the sample. As a verification, good correlation could be found between the illite/smectite content determined by  $\mu\text{-XRD}$  and the corresponding nickel concentrations (Fig. 10a,b).

For D11-U, Factor 4 contained uranium at the highest concentration, 400  $\mu\text{g/g}$ , accompanied with Ca, Mn and Fe as main elements. This finding is in accordance with the ring appearance and SEM/EDX measurements [40], that the mineral phase responsible for the strong uranium uptake was the ankerite rims surrounding dolomite grains. The presence of the ankerite rims could also be verified using micro-XRD (Figure 10c). The uranium binding capability was one order of magnitude higher compared to other mineral phases. Factor 1 related to the clayey matrix contained uranium at a concentration of less than 10  $\mu\text{g/g}$  (the average uranium load of the thin section was 20  $\mu\text{g/g}$ ).

The above results show a good performance of PMF, however, when the number of mineral phases present in the scanned area is large compared to the number of representative elements determined by  $\mu\text{-XRF}$ , the results obtained by PMF can be ambiguous.

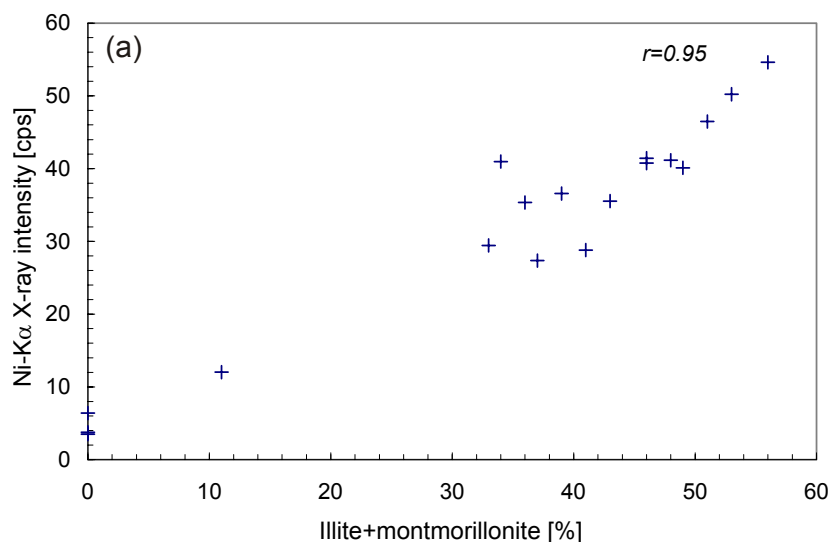


**Figure 10.** Micro-XRD results of selected positions, (a) scatter plot of illite and montmorillonite content versus  $\text{K}\alpha$  X-ray intensity on sample area D11-Ni, (b) diffractogram of a corresponding clay-rich position, and (c) diffractogram at a typical position at an U-rich ring, verifying the presence of ankerite on the sample area

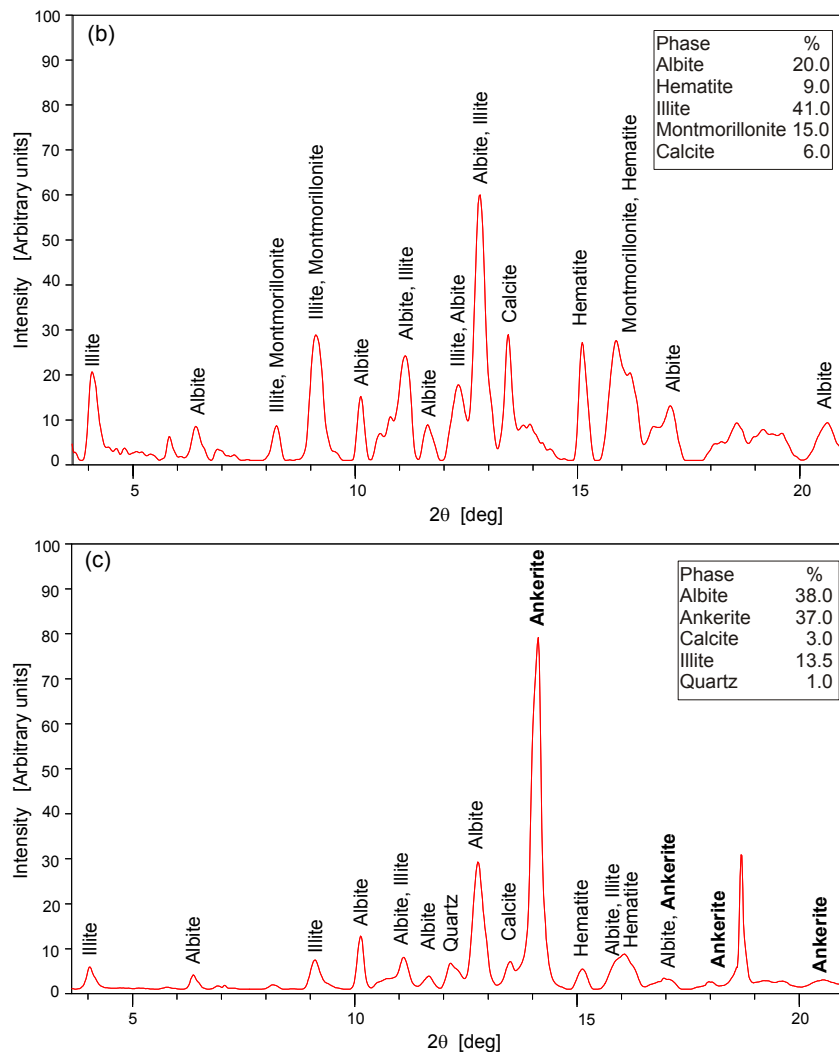


Figure 10. (continued)

### 3.4 Cluster analysis

By definition, multiple factors such as mineral phases can be present in the same pixel. It was the reason for applying the factorization approach for relation of abstract factors to mineral phases. Cluster analysis is a different approach, where one pixel can only belong to one cluster based on the main mineral phase present in the given pixel. Despite this fact, the method is capable to provide information on the ion uptake capacities of different main mineral phases.

For neither sample areas the number of clusters was chosen to be higher than the number of factors applied during PMF because it is sure that the sample does not contain more areas related to separable mineral phases (e.g. potassium feldspar, calcite) or mineral aggregations (clayey matrix). Only those elements were taken into account for cluster analysis which were dominant in the factors obtained as the result of PMF. It was necessary because elements with low X-ray intensity and large standard deviation might influence the results of CA.

The representative average composition of each cluster could be determined from the average of the characteristic intensities of the pixels classified to it. Results with less statistical error encumbered could be obtained if the intensities have been determined after summation of the X-ray spectra of pixels belonging to the same cluster by fitting of the sum spectra [22].

Before cluster analysis every variable was normalized to its maximum to take part with the same weight defined by the X-ray intensity of the chemical elements in the calculation of the distance between the objects. Continuously increasing the number of clusters the cluster distribution maps and the elemental composition of the factors were examined.

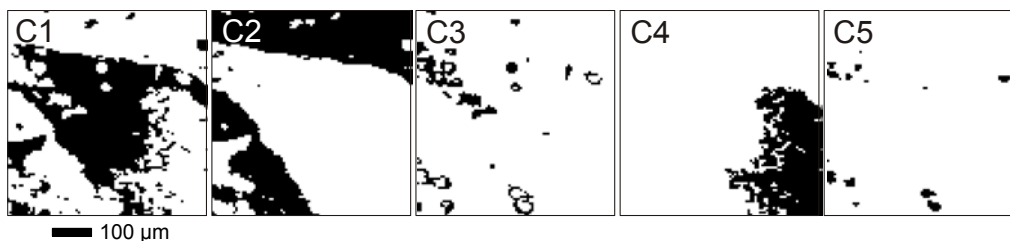


**Figure 11.** Cluster maps corresponding to the scanned area presented in Figure 6a. Black pixels are assigned to the given cluster.

During the evaluation of the scanned area presented in Fig. 6b (D-11 sample treated with  $\text{UO}_2^{2+}$ ), the number of clusters was fixed at the value of 5. Namely in this case the cluster distribution maps (Fig. 11) showed the best correspondence with the mineral phases occurring in the sample area. These mineral phases are potassium feldspar, carbonates and silicates (e.g.: albite, quartz; without detectable X-ray lines during  $\mu$ -XRF measurements carried out in air using 17.5 keV excitation energy). In addition the areas where potassium and iron consistently occurred at the same position were regarded as clayey matrix. In these areas besides layered silicates (mainly illite), 10–100 nm size hematite grains were present in the fine-grained base material [31]. Furthermore there was a separable phase which appeared on the edge of the calcium rich dolomites.

After the identification of the main mineral phases of each cluster the uranium binding capability of the phases could be calculated (Table 1). The assignment map of Cluster 3 contains the rings appearing on the elemental map of uranium, this cluster had an average uranium content of 40  $\mu\text{g/g}$ . It seems to be in contradiction with the PMF results indicating that ankerite could bind around 400  $\mu\text{g/g}$  uranium. However, micro-XRD results show that the ankerite content at pixels belonging to U-rich rings was 5–30%, the rest was albite, calcite and dolomite. Therefore the average uranium content of Cluster 3 was in accordance with the average ankerite content of the pixels assigned to it. Neighbouring pixels could also contain ankerite causing significant uranium intensity of Cluster 4 and Cluster 1, the latter representing Na-, Al-silicates (mainly albite and quartz). Cluster 2 which corresponds to the clayey matrix was found to be a significant uranium adsorbent. The number of pixels classified to this cluster was much higher than that of the ring phase therefore the value of the uranium intensity per pixel was much lower than that of Cluster 3. The average uranium concentration of Cluster 2 (8  $\mu\text{g/g}$ ) was found to be similar to the uranium concentration assigned to the factor representing the clayey matrix obtained by PMF. It means that pixels assigned to the clayey matrix cluster did not contain significant amount of minerals dominant in other clusters. Potassium feldspar corresponding to Cluster 5 did not bind the uranyl ion (see Table 1).

**Table 1.** Uranium  $\text{La}$  X-ray intensities and concentrations related to the clusters

Cluster number	Number of pixels	U-La intensity [cps/100 mA]	U-La intensity [%]	U-La intensity per pixel [cps/100 mA]	U concentration per pixel [ $\mu\text{g/g}$ ]
1	3040	2090	22	0.69	4.3
2	2937	3630	38	1.24	8.1
3	454	2820	30	6.21	40.4
4	135	710	7	5.24	34.8
5	1442	290	<3	0.19	1.3
Total	8008	9540	100	1.19	7.8

In relation to the whole area significant amount (30%) of uranium was bound to Cluster 3 related to the ankerite-rich regions corresponding to the uranium-rich rings. In case of every measured sample areas this phase was only a small part of the examined area namely only low number of pixels could be assigned to it. As a consequence the concentration of uranium per pixel was multiple of other mineral phases (Table 3). The above mentioned phase could be found dispersed generally in the sample so although it has subordinate role in the binding compared to the clayey matrix but its effect is not negligible.

#### 4. Conclusions

Micro-XRF elemental mapping itself contains sufficient information in order to identify the main mineral groups responsible for the uptake of different metal ions by clay-rich rocks. They are chemically identical to radioactive ions escaping from potential high level waste repositories. This approach is possible when the bulk mineral composition is known (e.g. from powder XRD) and XRF maps are evaluated by appropriate data handling.

The examination of pairwise elemental correlations is a useful tool in identifying the main groups of mineral phases responsible for the uptake, but it works well for simple cases, when one of them binds the majority amount of the element of interest. For every measured sample the intensity of Ni and Cs shows the most significant correlation with the clayey matrix that could be deduced by correlation between the given element and K as well as Fe. U and Nd was found to be bound not only to the clayey matrix, but the cavity filling minerals also played important role in the uptake.

Multivariate methods were found to be efficient tools for extracting information from the elemental distribution maps obtained by  $\mu$ -XRF both for the clayey matrix and fracture infilling regions. Conventional FA already delivered information on the possible mineral phases responsible for the uptake. By using positive matrix factorization as a new approach the factors with higher sorption capacity could be identified and with additional mineralogical information the uptake capacity of the different mineral phases could be quantified.

In case of Ni 170  $\mu\text{g/g}$  was bound to the factor representing the clayey matrix, in accordance with the clay content and the average load of 100  $\mu\text{g/g}$ . For U, a separate factor with the contribution map similar to the uranium map was formed, having high loading in Ca, Mn and Fe apart from U. This factor could be associated to ankerite  $[\text{Ca}(\text{Fe}^{2+}, \text{Mg}, \text{Mn})(\text{CO}_3)_2]$  mineral, which was verified by point  $\mu$ -XRD measurements. The uptake capacity of ankerite was estimated as 400  $\mu\text{g/g}$  U, much higher than the average U load of the sample (20  $\mu\text{g/g}$ ). CA was found to be capable of providing information on the ion uptake capacities of areas dominated by main mineral phases.

#### 5. Acknowledgements

The research leading to these results has received funding from the Swiss-Hungarian Cooperation Programme through Project n° SH/7/2/11. We acknowledge the Synchrotron Light Source ANKA for provision of instruments at their beamlines and we would like to thank Ábel Szabó for his great help in sample preparation. The courtesy of the Public Limited Company for Radioactive Waste Management (PURAM, Hungary) for providing the samples for analysis is also appreciated.

#### References

- [1] B. Baeyens, M.H. Bradbury. A mechanistic description of Ni and Zn sorption on Na-montmorillonite. 1. Titration and sorption measurements. *Journal of Contaminant Hydrology* 27 (1997) 199-222.
- [2] C. Poinssot, B. Baeyens, M.H. Bradbury. Experimental and modelling studies of caesium sorption on illite. *Geochimica et Cosmochimica Acta* 63 (1999) 3217-3227
- [3] M.H. Bradbury, B. Baeyens. A generalised sorption model for the concentration dependent uptake of caesium by argillaceous rocks. *Journal of Contaminant Hydrology* 42 (2000) 141-163.
- [4] C. Latrille, J. Ly, M. Herbette. Retention of Sn(IV) and Pu(IV) onto four argillites from the Callovo-Oxfordian level at Bure (France) from eight equilibrated sedimentary waters. *Radiochimica Acta* 94 (2006) 421-427
- [5] P. Mell, J. Megyeri, L. Riess, Z. Máthé, J. Csicsak, K. Lázár. Sorption of Co, Cs, Sr and I onto argillaceous rock as studied by radiotracers. *Journal of Radioanalytical and Nuclear Chemistry* 268 (2006) 405-410
- [6] E. Hartmann, H. Geckeis, T. Rabung, J. Lützenkirchen, T. Fanghänel. Sorption of radionuclides onto natural clay rocks. *Radiochimica Acta* 96 (2008) 699-707.
- [7] B.A. Powell, M.C. Duff, D.I. Kaplan, R.A. Fjeld, M. Newville, D.B. Hunter, P.M. Bertsch, J.T. Coates, P. Eng, M.L. Rivers, S.M. Serkiz, S.R. Sutton, I.R. Triay, D.T. Vaniman. Plutonium Oxidation and Subsequent Reduction by Mn(IV) Minerals in Yucca Mountain Tuff. *Environmental Science and Technology* 40 (2006) 3508-3514
- [8] E. Wieland, N. Mace, R. Dähn, D. Kunz, J. Tits. Macro- and micro-scale studies on U(VI) immobilization in hardened cement paste. *Journal of Radioanalytical and Nuclear Chemistry* 286 (2010) 793-800.

- 
- [9] R.D. Fröhlich, S. Amayri, J. Drebert, D. Grolimund, J. Huth, U. Kaplan, J. Krause, T. Reich. Speciation of Np(V) uptake by Opalinus Clay using synchrotron microbeam techniques. *Analytical and Bioanalytical Chemistry* 404 (2012) 2151-2162.
- [10] D.M. Singer, J.M. Zachara, G.E. Brown Jr. Uranium speciation as a function of depth in contaminated Hanford sediments - A micro-XRF, micro-XRD, and micro- and bulk-XAFS Study. *Environmental Science and Technology* 43 (2009) 630-636.
- [11] M.A. Denecke, K. Janssens, K. Proost, J. Rothe, U. Noseck. Confocal micrometer-scale X-ray fluorescence and X-ray absorption fine structure studies of uranium speciation in a tertiary sediment from a waste disposal natural analogue site. *Environmental Science and Technology* 39 (2005) 2049-2058.
- [12] C. Walther, M.A. Denecke, Actinide colloids and particles of environmental concern. *Chemical Reviews* 113 (2013) 995-1015.
- [13] M.A. Denecke, A. Somogyi, K. Janssens, R. Simon, K. Dardenne, U. Noseck. Microanalysis (micro-XRF, micro-XANES, and micro-XRD) of a tertiary sediment using microfocused synchrotron radiation. *Microscopy and Microanalysis* 13 (2007) 165-172.
- [14] T. Sudo, S. Shimoda, H. Yotsumoto, S. Aita, eds. *Electron Micrographs of Clay Minerals. Developments in Sedimentology Vol. 31.* Elsevier, 1981, p. 34.
- [15] F. Nieto, X. Arroyo. Microscopic methods. in: S. Fiore, J. Cuadros, F.J. Huertas, eds. *Interstratified clay minerals. Origin, characterization & geochemical significance.* Aipea Educational Series, DIGILABS, 2010, pp. 73-88
- [16] A. Somogyi, L. Vincze, K. Janssens, B. Vekemans, A. Rindby, F. Adams. Interpretation and use of inter-element correlation graphs obtained by scanning X-ray fluorescence micro-beam spectrometry from individual particles. Part I – theory. *Spectrochimica Acta Part B* 55 (2000) 75-89.
- [17] A. Somogyi, L. Vincze, K. Janssens, B. Vekemans, A. Rindby, F. Adams. Interpretation and use of inter-element correlation graphs obtained by scanning X-ray fluorescence micro-beam spectrometry from individual particles. Part II – application. *Spectrochimica Acta Part B* 55 (2000) 1039-1049.
- [18] L.H. Tecer, G. Tuncel, F. Karaca, O. Alagha, P. Süren, A. Zararsiz, R. Kirmaz. Metallic composition and source apportionment of fine and coarse particles using positive matrix factorization in the southern Black Sea atmosphere. *Atmospheric Research*, 118 (2012) 153-169
- [19] S. Karnae, K. John. Source apportionment of fine particulate matter measured in an industrialized coastal urban area of South Texas. *Atmos. Environ.* 45 (2011) 3769-3776
- [20] J.-F. Fabretti, N. Sauret, J.-F. Gal, P.-C. Maria, U. Schärer. Elemental characterization and source identification of PM<sub>2.5</sub> using Positive Matrix Factorization: the Malraux road tunnel, Nice, France. *Atmos. Res.* 94 (2009) 320-329
- [21] B. Vajna, G. Patyi, Zs. Nagy, A. Bódis, A. Farkas, Gy. Marosi. Comparison of chemometric methods in the analysis of pharmaceuticals with hyperspectral Raman imaging. *Journal of Raman Spectroscopy* 42 (2011) 1977-1986.
- [22] B. Vekemans, K. Janssens, L. Vincze, A. Aerts, F. Adams, J. Hertogen. Automated segmentation of  $\mu$ -XRF image sets. *X-Ray Spectrometry* 26 (1997) 333-346.
- [23] B. Vekemans, L. Vincze, F.E. Brenker, F. Adams. Processing of three-dimensional microscopic X-ray fluorescence data. *Journal of Analytical Atomic Spectrometry* 19 (2004) 1302-1308.
- [24] M. Lerotic, C. Jacobsen, T. Schäfer, S. Vogt. Cluster analysis of soft X-ray spectromicroscopy data. *Ultramicroscopy* 100 (2004) 35-57
- [25] P. Árkai, K. Balogh, A. Demény, I. Fórizs, G. Nagy, Z. Máthé. Composition, diagenetic and post-diagenetic alterations of a possible radioactive waste repository site: the Boda Albitic Claystone Formation, southern Hungary. *Acta Geol. Hung.* 43 (2000) 351-378.
- [26] A. Varga, Gy. Szakmány, B. Raucsik, Z. Máthé. Chemical composition, provenance and early diagenetic processes of playa lake deposits from the Boda Siltstone Formation (Upper Permian), SW Hungary. *Acta Geol. Hung.* 48 (2005) 49-68.
- [27] Z. Máthé, A. Varga. „Seasoning” to the palaeoenvironmental reconstruction of the Permian Boda claystone Formation: pseudomorphs after halit in the claystone samples of the deep drillings BAT-4. *Bulletin of the Hungarian Geological Society* 142 (2012) 201-204.
- [28] K. Lázár, Z. Máthé. Claystone as a potential host rock for nuclear waste storage. In: M. Valášková, G.S. Martynkova (eds). *Clay minerals in Nature – Their Characterization, Modification and Application.* Intech, 2012, pp. 56-80. ISBN 978-953-51-0738-5; DOI: 10.5772/48123
- [29] A. Varga, B. Raucsik, Gy. Szakmány, Z. Máthé. Mineralogical, petrological and geochemical characteristics of the siliciclastic rock types of Boda Siltstone Formation. *Bulletin of the Hungarian Geological Society* 136 (2006) 201-232.

- 
- [30] P. Sipos, T. Németh, Z. Máthé. Preliminary results on the Co, Sr, and Cs sorption properties of the analcime-containing rock type of the Boda Siltstone Formation. *Central European Geology*, 53 (2010) 67-78.
- [31] T. Németh, A. Demény. Detailed mineralogical study of samples of Boda Siltstone Formation (BSF). Research report, Hungarian Academy of Sciences Institute for Geochemical Research, Budapest, 2011, 35 p.
- [32] Gy. Konrád, K. Sebe, A. Halász, E. Babinszki. Sedimentology of a Permian playa lake: the Boda Claystone Formation, Hungary. *Geologos* 16 (2010) 27-41.
- [33] B. Vekemans, K. Janssens, L. Vincze, F. Adams, P. Van Espen, Analysis of X-ray spectra by iterative least squares (AXIL): New developments, *X-Ray Spectrom.* 23 (1994) 278–285
- [34] W. De Nolf, K. Janssens. Micro X-ray diffraction and fluorescence tomography for the study of multilayered automotive paints. *Surface and Interface Analysis* 42 (2010) 411-418.
- [35] I.E. Sajó. Powder Diffraction Phase Analytical System, Version 3.0, Users Guide, Budapest, 2005
- [36] I. Bondarenko, B. Treiger, R. Van Grieken, P. Van Espen. IDAS: A Windows based software package for cluster analysis. *Spectrochimica Acta Part B* 51 (1996) 441–456.
- [37] D. L. Massart, L. Kaufman. The interpretation of analytical chemical data by the use of cluster analysis, Canada, 1983
- [38] G. Norris, R. Vedantham: EPA Positive Matrix Factorization (PMF) 3.0 Fundamentals & UserGuide, 2008, U.S. Environmental Protection Agency Office of Research and Development, Washington
- [39] <http://webmineral.com/>
- [40] D. Breitner, J. Osán, M. Fábrián, P. Zagyvai, C. Szabó, R. Dähn, M. Marques, I. Sajó, Z. Máthé, S. Török. Effect of mineralogical characteristics on the U(VI) uptake of Boda Claystone Formation as the candidate host rock of high activity and long lived nuclear waste repository in Hungary. Submitted to *Environmental Earth Sciences*